Electronic Supplementary Material (ESI) for Energy & Environmental Science.

Supplementary Information

Hybrid thermo-electrochemical conversion of plastic wastes commingled with marine biomass to value-added products using renewable energy

Jonah M. Williams[a], Michael P. Nitzsche[b], Lev Bromberg[b], Zifeng Qu[c], Aaron J. Moment[c], T. Alan Hatton[b] and Ah-Hyung Alissa Park[a,c,d,§]

[a]Department of Earth and Environmental Engineering, Columbia University, New York. New York, 10027
[b]Department of Chemical Engineering, Massachusetts Institute of Technology, Cambridge, Massachusetts, 02138
[c]Department of Chemical Engineering, Columbia University, New York. New York, 10027
[d]Lenfest Center for Sustainable Energy, Columbia University, New York. New York, 10027

[§]ap2622@columbia.edu

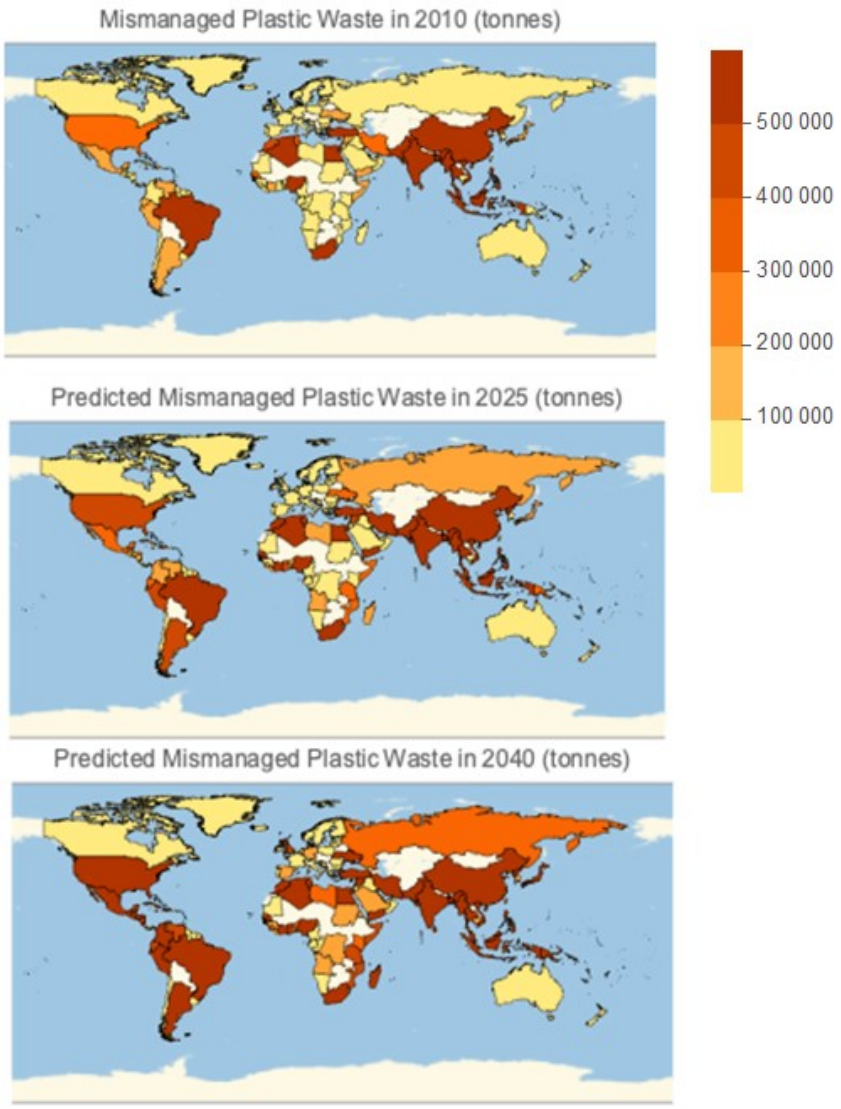

Figure S1. Graphic depiction of mismanaged plastic waste in total tonnes from 2010 (actual) until 2040 (predicted) from 192 coastal countries around the globe. Coastal mismanaged plastic waste is projected to grow with both population and industrialization, seeing a greater contribution from Asia, South America, and North America in 2040. Data adapted from Jambeck et al.[1]

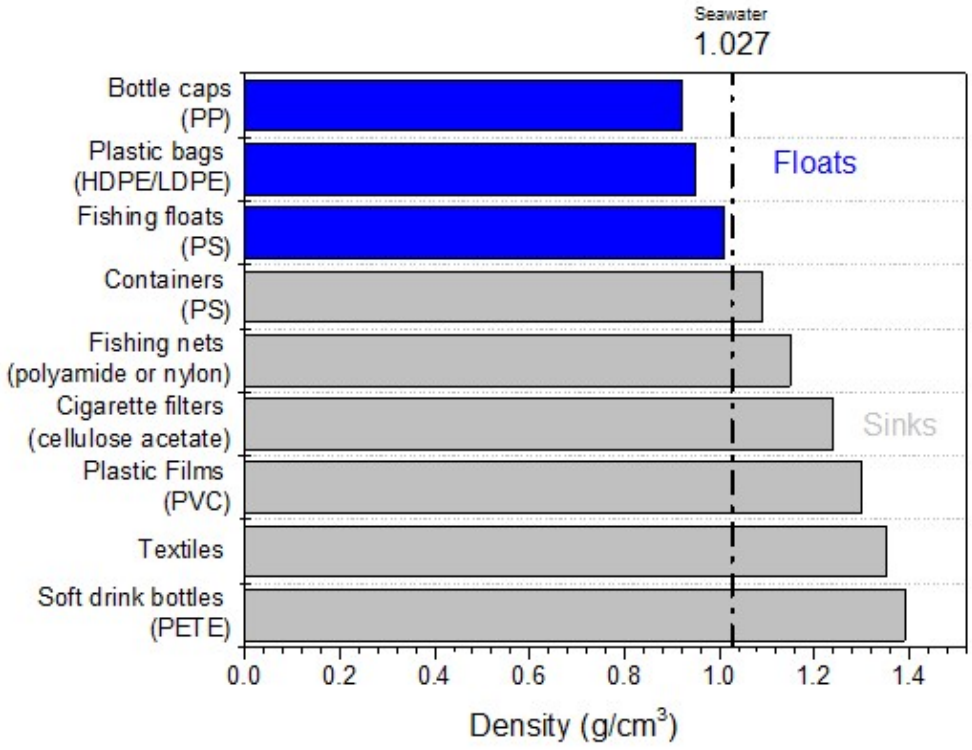

Figure S2. Studied densities of common marine plastic wastes relative to that of the average density of surface seawater. The surface plastic layer consists principally of PP, PE, and a certain fraction of PS in the form of bottles, bottle caps, and fishing gear. However, contamination of marine plastics with other ocean debris and biomass can alter their buoyancy, leading to a potential increase in surface plastic due to agglomeration.[2,3]

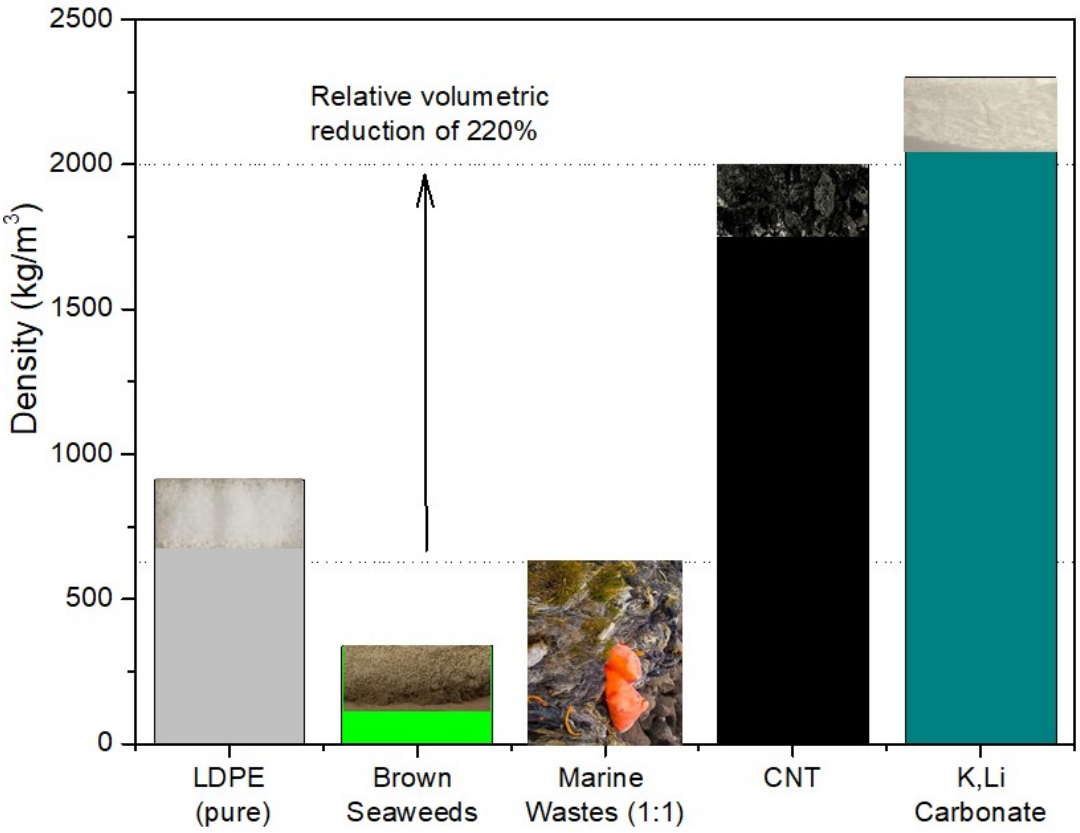

Figure S3. Volumetric reduction of the commingled biomass and plastic wastes towards the desired higher value intermediate products (lithium and potassium carbonate) and the final carbon product, carbon nanotubes (CNTs) via the proposed thermo-electrochemical molten salt processing scheme. A relative volume reduction of 220% is achieved from the feedstock reducing the size of the waste and producing a high value, high carbon commodity (CNTs) in the process.

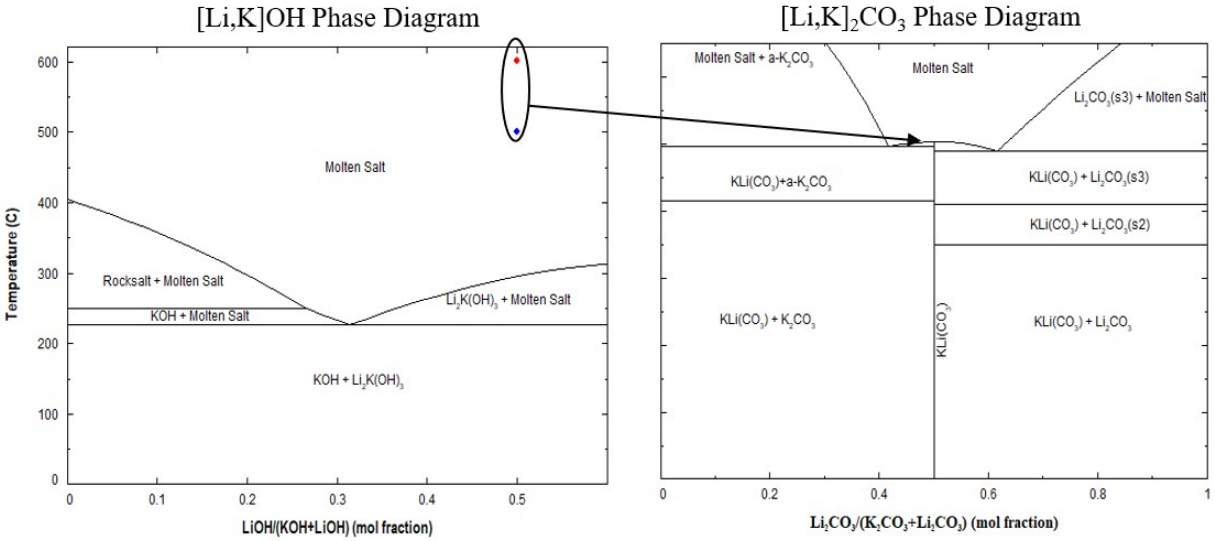

Figure S4. Phase diagram of a mixture of LiOH and KOH as a function of mole fraction LiOH (left image) and phase diagram of a mixture of Li_2CO_3 and K_2CO_3 as a function of mole fraction Li_2CO_3 (right image). The molar mixture of 1:1 LiOH:KOH was chosen such that it would theoretically yield a eutectic carbonate flux during the tandem thermo-electrochemical conversion process. Images and data were obtained and modified from the FTSalt - FACT Salt Phase Diagram Database from Factsage.[4] Blue and red dots indicated studied ATT reaction temperatures.

Figure S5. Schematic and photographs of the reactor CO_2 electrolysis.

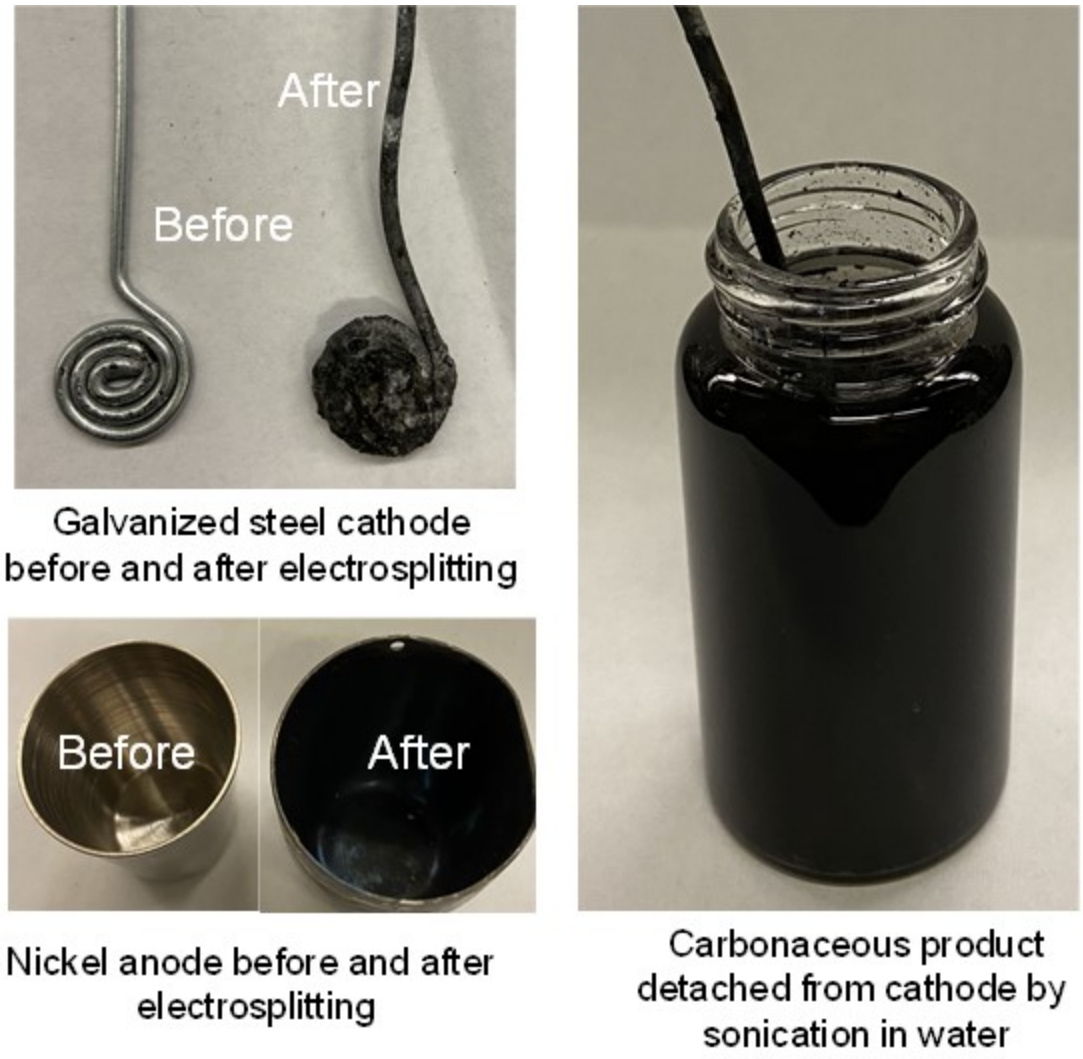

Figure S6. Photographs showing the results of the CO_2 electrolysis in eutectic carbonate/LiOH blends. Pictured are galvanized steel cathode before and after electrolysis, nickel anode before and after electrolysis, and a suspension of carbonaceous product in water obtained by sonication of the cathode that underwent electrolysis.

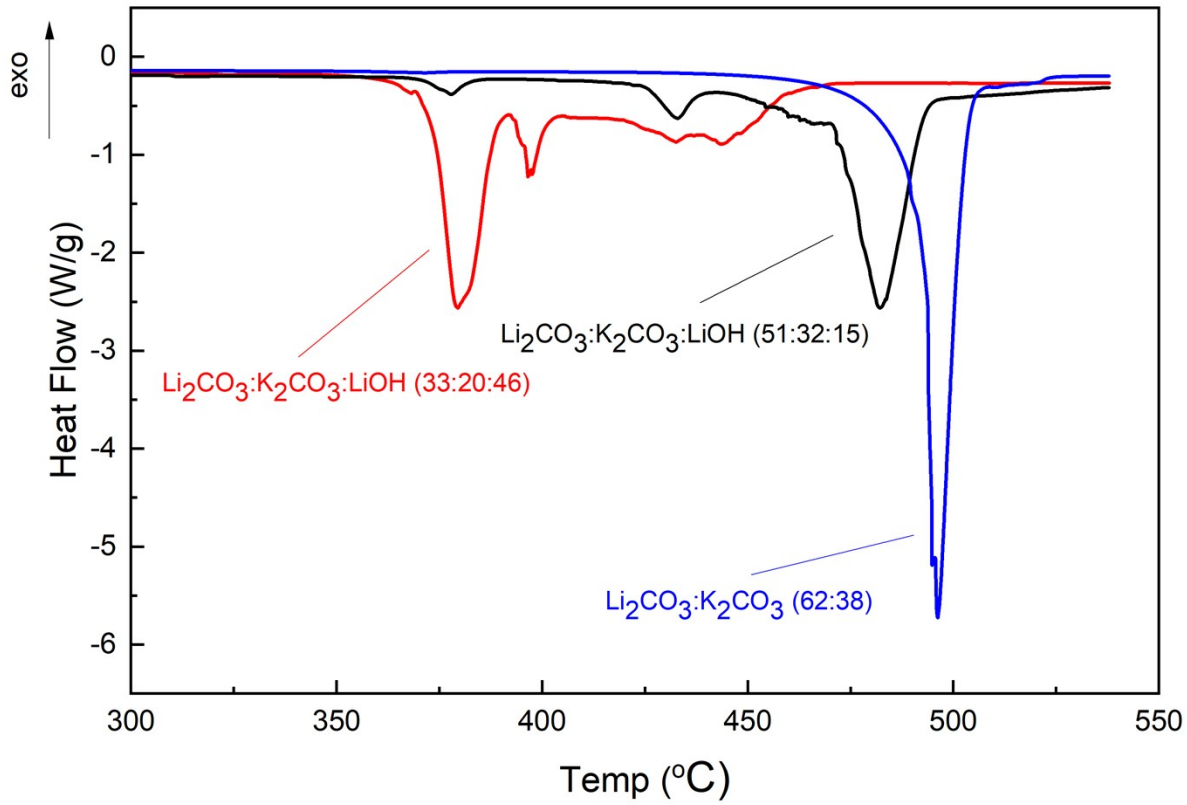

Figure S7. Thermogravimetric analysis of representative Li_2CO_3/K_2CO_3/LiOH compositions in nitrogen. Numbers indicate component's content in mol%. Heating rate, 10 °C/min.

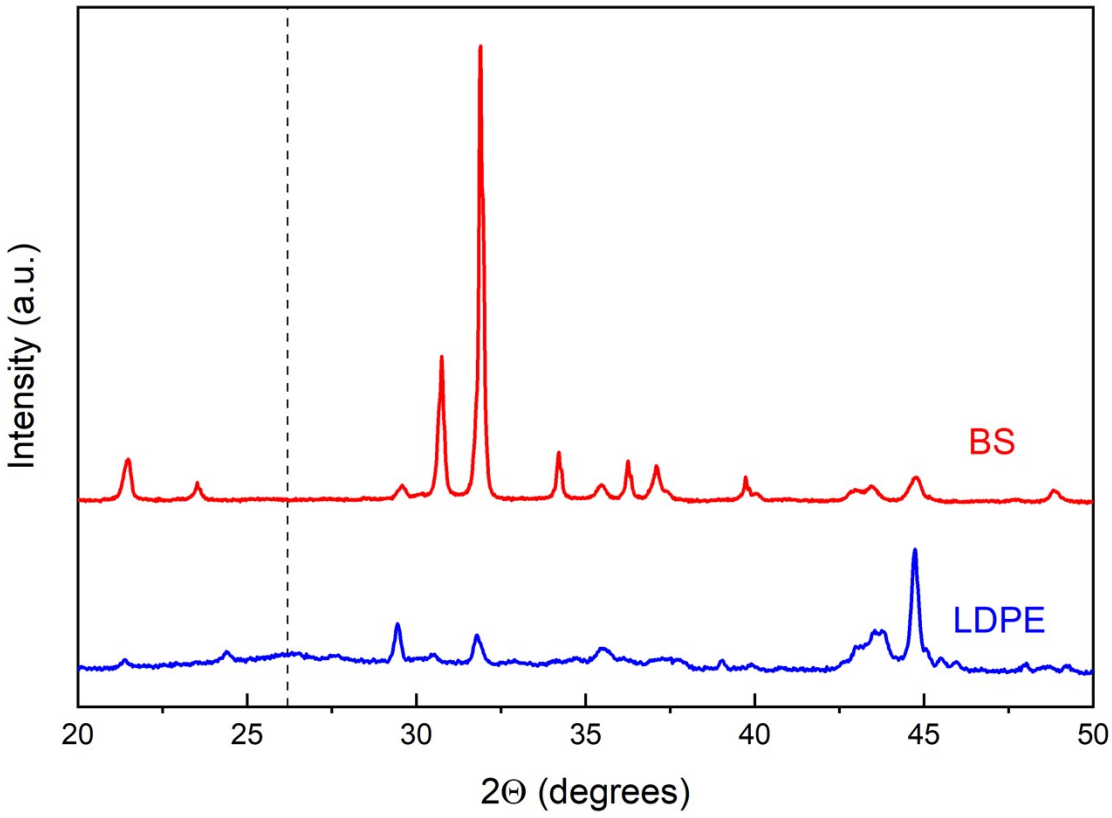

Figure S8. Representative XRD patterns of the products of CO_2 electrolysis conducted at 550 °C in molten Li, K carbonate/LiOH blend (initial electrolyte composition, Li_2CO_3:K_2CO_3:LiOH, 52:32:15 molar ratio. Cathode: galvanized steel, anode: Ni crucible. Current density on the cathode during electrolysis: 120 mA/cm^2. For other conditions, see main text. Dotted vertical line shows graphitic peaks at 26.2°.

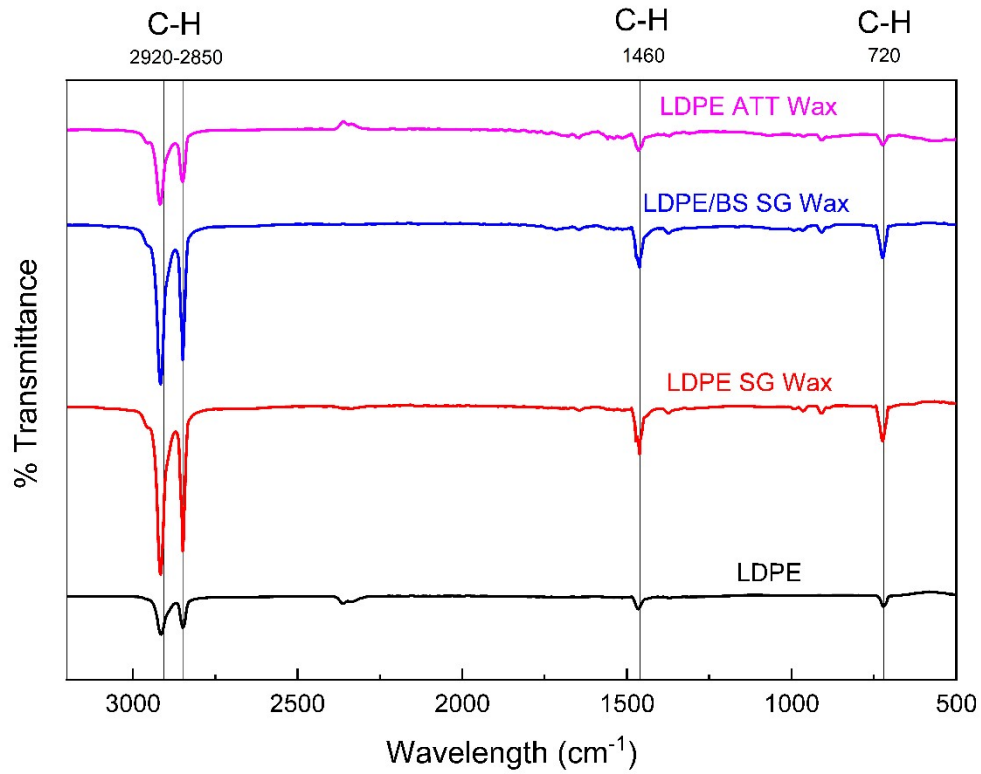

Figure S9. Fourier transform infrared spectroscopy (FTIR) transmittance spectra of various waxes produced as considerable products during the SG of LDPE, the SG of LDPE and BS, and the ATT of LDPE, all with reference to the original LDPE feedstock. C-H vibrational peaks were highlighted at 2929-2850, 1460, and 720 cm^{-1}.[5,6]

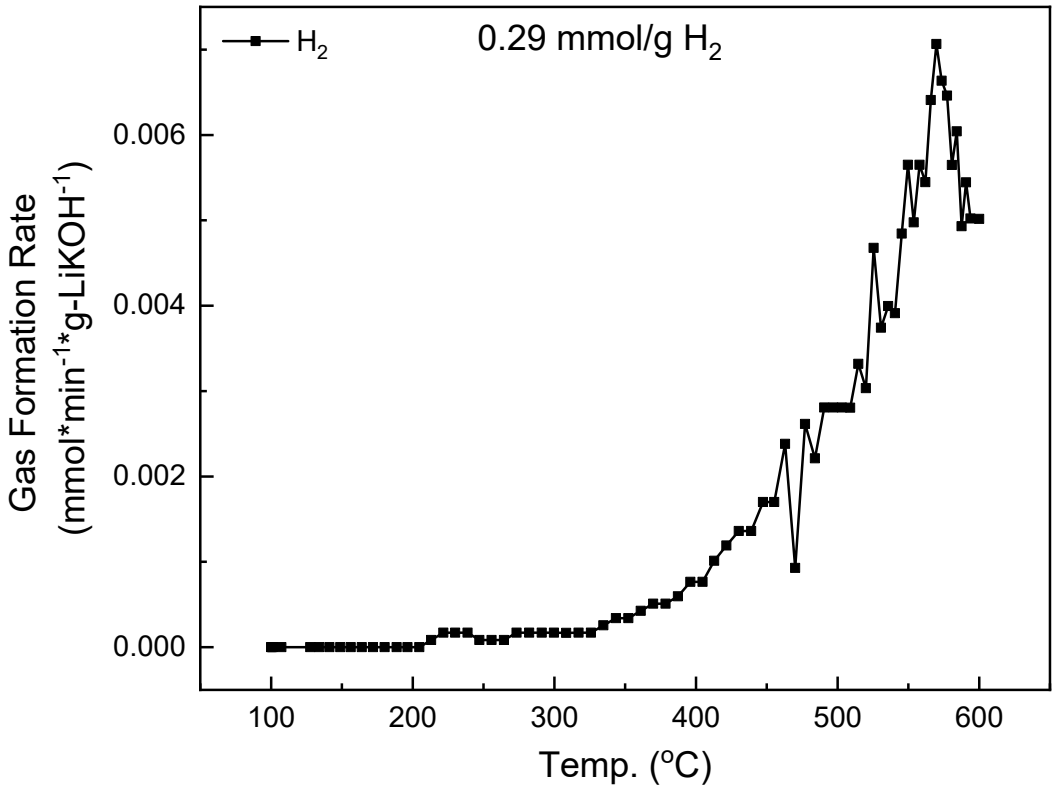

Figure S10. Hydrogen evolution data for a control experiment done with the eutectic K-Li hydroxide without any biomass or LDPE.

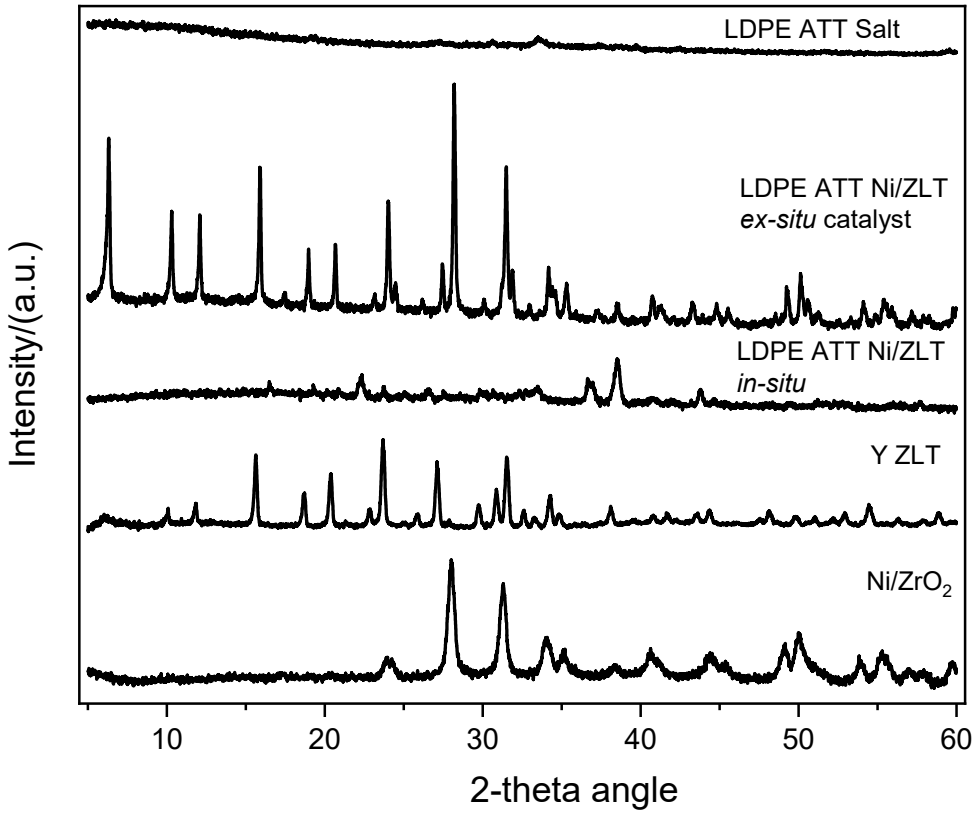

Figure S11. PXRD spectral data (from top to bottom) of the raw Ni/ZrO_2 and Y-zeolite catalysts and the salts of the LDPE ATT with Ni/ZLT *in-situ*, the spent catalyst from LDPE ATT Ni/ZLT *ex-situ*, and the mostly amorphous LDPE ATT salt product.

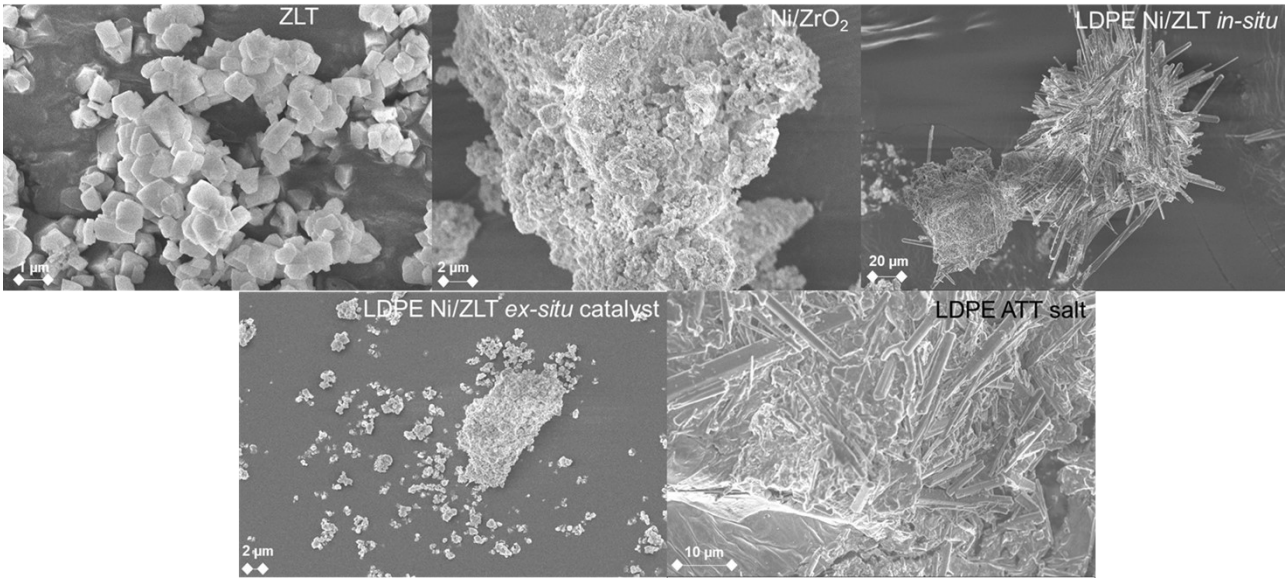

Figure S12. SEM micrographs (from left to right) of the raw Ni/ZrO_2 and Y-zeolite catalysts and the salts of the LDPE ATT with Ni/ZLT *in-situ*, the spent catalyst from LDPE ATT Ni/ZLT *ex-situ*, and the mostly amorphous LDPE ATT salt product.

Table S1. Physical parameters calculated from the corresponding Differential Scanning Calorimetry (DSC) curves including crystallization temperature (T_c), melting temperature (T_m), enthalpy of crystallization (ΔH_c), enthalpy of melting (ΔH_m), and percent crystallinity (X_c).[7]

Physical Property	LDPE Control	LDPE SG Wax	LDPE/BS SG Wax	LDPE/BS ATT Wax
Crystallization Temp., T_c (°C)	93.0 ± 0.0	76.3 ± 0.7	76.6 ± 0.1	83.2 ± 0.1
Melt Temp., T_m (°C)	110.8 ± 0.8	84.3 ± 0.5	84.1 ± 0.3	88.9 ± 0.3
Enthalpy of Crystallization, ΔH_c (J/g)	165.8 ± 4.5	152.9 ± 0.0	164.2 ± 1.8	169.4 ± 1.4
Enthalpy of Melting, ΔH_m (J/g)	-161.9 ± 6.0	-141.4 ± 4.6	-158.9 ± 2.0	-178.8 ± 1.9
Percent Crystallinity*, X_c (%)	55.2	48.3	54.2	61.0

*Percent crystallinity references the pure melting properties of 100% crystalline LDPE.

Table S2. Physical data extracted from the High Temperature Gel Permeation Chromatography (HT-GPC) curves showing key parameters such as column retention time (min), peak area (mV per sec.), the number average molecular weight (Mn), the weight average molecular weight (Mw), the higher average molecular weights (Mz), and the polydispersity index (Mw/Mn).

	LDPE Control	**LDPE SG Wax**	**LDPE/BS SG Wax**	**LDPE/BS ATT Wax**	**LDPE ATT Salt**
Retention Time (min)	10.417	12.74	12.727	12.648	12.96
Area (mV per sec.)	476.198	764.67	485.609	480.999	98.45
Mn	154088	8909	8996	10528	7093
Mw	555488	10366	11733	13226	11304
Mz	1761253	12102	17125	18619	16775
Mw/Mn	3.605	1.164	1.304	1.256	1.594
Mz/Mw	3.171	1.168	1.46	1.408	1.484
Start Molecular Mass	1.34E+07	56403	119183	160381	44772
Top Molecular Mass	299420	9677	9910	11372	6451
End Molecular Mass	12791	2697	1873	2697	1653

References:

1 J. R. Jambeck, R. Geyer, C. Wilcox, T. R. Siegler, M. Perryman, A. Andrady, R. Narayan and K. L. Law, *Science (80-.).*, 2015, **347**, 768–771.

2 Density of plastic, https://www.statista.com/statistics/595434/plastic-materials-density/, (accessed 11 March 2021).

3 R. C. Thompson, C. J. Moore, F. S. V. Saal and S. H. Swan, *Philos. Trans. R. Soc. B Biol. Sci.*, 2009, 364, 2153–2166.

4 C. W. Bale, E. Belisle, P. Chartrand, S. . Decterov, G. Eriksson, A. E. Gheribi, K. Hack, I. H. Jung, Y. B. Kang, J. Melancon, A. D. Pelton, S. Petersen, C. Robelin, J. Sangster and M.-A. van Ende, *Calphad*, 2106, **54**, 35–53.

5 M. Arabiourrutia, G. Elordi, G. Lopez, E. Borsella, J. Bilbao and M. Olazar, *J. Anal. Appl. Pyrolysis*, 2012, **94**, 230–237.

6 J. V. Gulmine, P. R. Janissek, H. M. Heise and L. Akcelrud, *Polym. Test.*, 2002, **21**, 557–563.

7 Crystallinity / Degree of Crystallinity, https://www.netzsch-thermal-analysis.com/en/contract-testing/glossary/crystallinity-degree-of-crystallinity/, (accessed 11 March 2021).